Environmental Technology & Innovation 27 (2022) 102747

Contents lists available at ScienceDirect

Environmental Technology & Innovation

journal homepage: www.elsevier.com/locate/eti

Interfacial Ni active sites strike solid solutional counterpart in CO_2 hydrogenation

Ákos Szamosvölgyi [a], T. Rajkumar [a], András Sápi [a,b,*], Imre Szenti [a], Marietta Ábel [a], Juan Fernando Gómez-Pérez [a], Kornélia Baán [a], Zsolt Fogarassy [c], Erzsébet Dodony [c], Béla Pécz [c], Seema Garg [e], János Kiss [a,d], Ákos Kukovecz [a], Zoltán Kónya [a,d]

[a] University of Szeged, Interdisciplinary Excellence Centre, Department of Applied and Environmental Chemistry, H-6720, Rerrich Béla tér 1, Szeged, Hungary

[b] Institute of Environmental and Technological Sciences, University of Szeged, H-6720, Szeged, Hungary

[c] Centre for Energy Research, Institute of Technical Physics and Materials Science, H-1121, Budapest, Hungary

[d] MTA-SZTE Reaction Kinetics and Surface Chemistry Research Group, University of Szeged, H-6720, Szeged, Hungary

[e] Department of Chemistry, Amity Institute of Applied Sciences, Amity University, Noida, India

ARTICLE INFO

Article history:
Received 30 July 2021
Received in revised form 11 April 2022
Accepted 5 June 2022
Available online 17 June 2022

Keywords:
CO_2 activation
Heterogeneous catalysis
Interface design
Solid solutions
Cerium-oxide

ABSTRACT

Ni enhanced CeO_2 based catalysts were tested in CO_2 hydrogenation reaction with the objective to investigate the importance and role of Ni^0 and Ni^0-NiO-CeO_{2-x} interfaces. Two materials were prepared: a 4 mol% NiO/CeO_2 interfacial oxide where CeO_2 supports NiO nanoparticles was produced by wet impregnation method and a $Ce_{0.96}Ni_{0.04}O_2$ mixed oxide was obtained by co-precipitation of Ce^{3+} and Ni^{2+} ions. Besides these materials, pure NiO and CeO_2 were also synthesized and tested, serving as reference materials. HRTEM, TPR, XRD, BET, EDS, Raman spectroscopy, and XPS were used for the characterization of the catalysts. The activity and selectivity strongly depended on metallic Ni content, which is tunable by the temperature of hydrogen pretreatment. The impregnated catalyst with significant metallic content exhibited high activity and high methane selectivity. The mixed oxide was more resistant to reduction, in the case of both the Ni^{2+} and Ce^{4+} species, thus it has low activity with high CO selectivity. The activity and methane selectivity increased considerably by increasing the metal content or higher hydrogen pretreatment temperature. *Operando* DRIFTS experiments suggested that bicarbonate and formate intermediates play important role in CO_2 hydrogenation in both types of catalysts. The reduced Ni particles help to produce the high amount of hydrogen needed for the hydrogenation of formate to methane. It turned out that the metallic Ni not only catalyzes the methane production from formate but also the bicarbonate-formate transformation. The most important factor in the high performance of these catalysts is the Ni^0/NiO ratio in the Ni^0-NiO-CeO_{2-x} interface.

* Corresponding author at: University of Szeged, Interdisciplinary Excellence Centre, Department of Applied and Environmental Chemistry, H-6720, Rerrich Béla tér 1, Szeged, Hungary.
E-mail address: sapia@chem.u-szeged.hu (A. Sápi).

https://doi.org/10.1016/j.eti.2022.102747

1. Introduction

Catalytic CO_2 hydrogenation is a promising method to reduce anthropogenic CO_2 in the atmosphere and also produce value-added liquid fuels and feedstock chemicals for the chemical industry (Centi et al., 2013; Sápi et al., 2019a,b; Wang et al., 2011). CO_2 conversion using H_2 produced from electrolysis of water powered by wind or solar energy produces carbon monoxide (CO), methane (CH_4), methanol (CH_3OH), and other valuable chemical feedstock. This approach is considered to be promising to reduce the atmospheric concentration of CO_2 (Porosoff et al., 2016). Because of the chemical inertness and thermodynamic stability of CO_2, efficient and selective CO_2 conversion remains a challenge (Freund and Roberts, 1996; Kiss et al., 2019; Zheng et al., 2017). Another route for CO_2 conversion is the production of CO. The produced CO can be used as feedstock in the Fischer–Tropsch (FT) process to transform value-added chemicals or fuels (Daza and Kuhn, 2016; Luk et al., 2017). Synthesis of methane or synthesis gas over the other products through CO_2 hydrogenation requires relatively low temperature and takes place at atmospheric pressure. Various transition metals such as Co, Ni, Ru, Rh, Pt, and Pd supported on metal oxides such as Al_2O_3, TiO_2, SiO_2, ZrO_2, and CeO_2 have been investigated for CO_2 methanation reaction (Frontera et al., 2017; Sápi et al., 2018; Vogt et al., 2018; Wang et al., 2016). Likewise, for water gas shift reaction transition metals such as Cu, Pt and Rh supported on various oxides such as Al_2O_3, TiO_2, SiO_2, ZrO_2, and CeO_2 have been investigated (Daza and Kuhn, 2016). CeO_2 has been extensively used as a support due to its redox behavior and oxygen storage capacity (OSC) (Montini et al., 2016). The OSC of CeO_2 derives from the oxygen deficiency of the crystal lattice, which is a desirable trait of metal oxides concerning catalysis (Zu et al., 2019). However, the stoichiometry and physical chemical properties of CeO_2 change at high temperatures, resulting in decreased OSC and subsequent deactivation. Recently different ceria based solid solutions and ceria with interfacial particles were engineered and tested for CO_2 hydrogenation (Rajkumar et al., 2021). To improve catalytic activity and thermal stability, CeO_2 is doped with various metals such as Mn, Fe, Co, Ni, Cu, or Zr (Li et al., 2016; Selvamani et al., 2015; Zhang et al., 2018b; Zhou et al., 2010). CeO_2 supported NiO has been reported as an excellent catalyst for various reactions such as oxidation of methane and selective catalytic reduction (SCR) of NO_x with NH_3 compared to pure CeO_2 due to the synergetic effect between the CeO_2 and NiO (Maitarad et al., 2014; Zhang et al., 2018b). The metal-support interface is crucial in determining product selectivity (Sápi et al., 2019a,b; Zhang et al., 2018a). A fundamental understanding of the difference between interfacial and solid solution effects on CO_2 hydrogenation at the atomic level is necessary. In this study, the difference between interfacial and solid solution effect on CO_2 hydrogenation over NiO impregnated CeO_2 (labeled as 4 mol% NiO/CeO_2 and $Ce_{0.96}Ni_{0.04}O_2$ solid solution catalysts have been studied.

2. Materials and methods

2.1. Catalyst synthesis

2.1.1. Chemicals

$Ce(NO_3)_3{\cdot}6H_2O$ and NaOH were obtained from Sigma-Aldrich. $Ni(NO_3)_2{\cdot}\ 6H_2O$ was obtained from Merck. All the chemicals were used without further purification. Distilled water was used for all synthesis and washing processes.

2.1.2. Synthesis of $Ce_{0.96}Ni_{0.04}O_2$ solid solution

The Ni^{2+} doped CeO_2 based solid solutions were prepared by the hydrothermal method according to the literature (Zhang et al., 2018a). In a typical synthesis, an appropriate amount of $Ce(NO_3)_3{\cdot}6H_2O$ and $Ni(NO_3)_2{\cdot}6H_2O$ were dissolved in distilled water. Then, NaOH solution was added dropwise into the solution until the pH reached 12. The obtained suspension was stirred constantly for 2 h before transferring into an autoclave, then kept at 200 °C for 24 h. When the hydrothermal reaction was finished, the product was washed with distilled water and dried in an oven at 80 °C overnight. Pure CeO_2 and NiO were also prepared with the same method.

2.1.3. Synthesis of NiO impregnated CeO_2

CeO_2 supported NiO with 4 mol% loading was prepared by wet impregnation method. In a typical synthesis, an aqueous solution containing an appropriate amount of $Ni(NO_3)_2{\cdot}6H_2O$ was added dropwise to the CeO_2 support. The excess water was removed at 80 °C under magnetic stirring. The obtained sample was further dried in an oven at 80 °C overnight and calcined at 400 °C for 2 h in air.

2.2. Sample characterization

2.2.1. N_2 adsorption–desorption isotherm measurements

The specific surface area (BET method), the pore size distribution, and the total pore volume were determined by the BJH method using a Quantachrome NOVA 2200 surface analyzer by N_2 gas adsorption/desorption at −196 °C. Before the measurements, the samples were pretreated in vacuum (< ∼0.1 mbar) at 200 °C for 2 h. Results are shown in the Supplementary Information.

2.2.2. Powder X-ray diffraction (XRD)

XRD studies of all samples were performed on a Rigaku MiniFlex II instrument with a Ni-filtered Cu-Kα source in the range of 2θ = 20-80°. Diffraction data are shown in the Supplementary Information. The XRD patterns of pure CeO_2, $Ce_{0.96}Ni_{0.04}O_2$, 4 mol% NiO/CeO_2, and NiO catalysts are shown in Fig. S3 of the Supplementary Information. Also, the XRD patterns of the spent catalysts are shown in Fig. S8 of the Supplementary Information.

2.2.3. Transmission electron microscopy (TEM)

Imaging of the synthesis products was carried out using a FEI TECNAI G2 20 X-Twin high-resolution transmission electron microscope operating at an accelerating voltage of 200 kV. The samples were drop-cast onto carbon film coated copper grids from ethanol suspension. The TEM images are shown in the Supplementary Information.

2.2.4. High angle annular dark field imaging (HAADF) and energy dispersive X-ray spectroscopy (EDX)

Pretreated catalyst samples were further investigated with a Thermo Fisher Scientific Themis TEM instrument equipped with Super-X EDX detectors. HAADF and EDX images were taken in STEM mode.

2.2.5. Raman spectroscopy

The Raman spectra were collected on a Bruker Senterra II equipped with a 532 nm wavelength laser source. The Raman spectra of pure CeO_2, $Ce_{0.96}Ni_{0.04}O_2$, 4 mol% NiO/CeO_2, and NiO catalysts are shown in Fig. S4 of the Supplementary Information.

2.2.6. H_2-temperature programmed reduction (H_2-TPR)

The temperature-programmed reduction (TPR) was carried out in a BELCAT-A analyzer using a reactor (quartz tube with 9 mm outer diameter) that was externally heated. Before the measurements, 50 mg of catalyst was pretreated in oxygen at 400 °C for 30 min and in N_2 at 400 °C for 15 min. Thereafter, the sample was cooled in flowing N_2 to 50 °C. The oxidized sample was flushed with N_2 containing 10% H_2, the reactor was heated linearly at a rate of 10 °C/min from 50 °C to 500 °C and the H_2 consumption was detected by a thermal conductivity detector (TCD). The result is showcased in section 6. of the Supplementary Information.

2.2.7. Energy-dispersive X-ray spectroscopy (EDS)

A field emission scanning electron microscope (Thermo Fisher Scientific Apreo C) equipped with an energy dispersive detector was used to characterize the elemental content of samples. The applied voltage was 20 kV and the spot size was 8. The data are presented in Table S2 of the Supplementary Information.

2.2.8. Operando diffuse reflectance infrared Fourier transform spectroscopy (DRIFTS)

Infrared spectroscopy measurements were carried out with an "Agilent Cary-670" Fourier transform infrared (FTIR) spectrometer equipped with a "Harrick Praying Mantis" diffuse reflectance attachment. The sample holder had two BaF_2 windows in the infrared path. The spectrometer was purged with dry nitrogen. The spectrum of the pretreated catalyst was used as background. At room temperature, a CO_2 to H_2 mixture with a molar ratio of 1:4 was introduced into the DRIFTS cell. The tubes were externally heated to avoid condensation. The catalyst was heated under the reaction feed linearly from room temperature to 400 °C, with a heating rate of 20 °C/min, and IR spectra were measured at 50 °C intervals.

2.2.9. In situ and ex situ X-ray Photoelectron Spectroscopy

The *in situ* X-ray photoelectron spectroscopy (XPS) measurements were performed in a Kratos Analytical XSAM800 instrument. Pretreatment and *in situ* sample preparations were done in the modified pre-chamber of the instrument. Pretreatment consisted of a cycle of oxidation (O_2, 1 atm, 300 °C, and 30 min) and reduction (H_2, 1 atm, 300 °C, 60 min). After this, the samples were introduced into the chamber to acquire spectra. Finishing data acquisition, CO_2 and H_2 (1:4 ratio) were introduced to the pre-chamber. The reaction time was 30 min at 400 °C and 1 atm. Thereafter spectra were collected once again. Also, the spent catalysts were removed from the quartz tube after cooling and were prepared for *ex situ* XPS. The data are presented in Fig. S11 of the Supplementary Information.

2.2.10. Hydrogenation of carbon dioxide in a continuous flow reactor

Before the catalytic reactions, the as-received catalysts were oxidized in O_2 atmosphere at 300 °C for 30 min to remove the surface contaminants and thereafter were reduced in H_2 at 300 °C for 60 min. In parallel, the samples were tested with 600 °C pre-reduction temperature also. Catalytic reactions were conducted at atmospheric pressure in a fixed-bed continuous-flow reactor (200 mm long with 8 mm id.), which was heated externally. The dead volume of the reactor was filled with quartz beads. The operating temperature was controlled by a thermocouple placed inside the oven close to the reactor wall. The samples were prepared as small fragments (about 1 mm) of slightly compressed pellets. Typically, the reactor filling contained 150 mg of the catalyst sample. In the reacting gas mixture molar ratio of CO_2: H_2 was 1:4 in all cases. The CO_2: H_2 mixture was fed with the help of mass flow controllers (Aalborg), and the total flow rate was 40 ml/min. The reacting gas mixture flow entered and left the reactor through externally heated tubing to avoid condensation. The

Table 1
Oxidation state distribution of Ce and Ni in pretreated and spent catalyst samples of 4 mol% NiO/CeO_2 and $Ce_{0.96}Ni_{0.04}O_2$

Samples	Ce^{3+}	Ce^{4+}	Ce^{3+}/Ce^{4+}	Ni^0	Ni^{2+}	Ni^0/Ni^{2+}
4 mol% NiO/CeO_2 after pretreatment	18.66%	81.32%	0.23	32.01%	67.99%	0.47
4 mol% NiO/CeO_2 after reaction	26.93%	73.06%	0.37	77.03%	22.97%	3.35
$Ce_{0.96}Ni_{0.04}O_2$ after pretreatment	21.48%	78.52%	0.27	0.0%	100%	–
$Ce_{0.96}Ni_{0.04}O_2$ after reaction	15.43%	84.57%	0.18	36.69%	63.31%	0.58

analysis of the products and reactants was performed with an Agilent 6890N gas chromatograph using an HP-PLOTQ column. The gases were detected simultaneously by thermal conductivity (TC) and flame ionization detectors (FID). The CO_2 was transformed by a methanizer into methane and it was also analyzed by FID. CO_2 conversion was calculated from carbon balance:

$$CO_2 \text{ conversion } (\%) = \frac{CO_{2\ \text{inlet}} - CO_{2\ \text{outlet}}}{CO_{2\ \text{inlet}}} \times 100\%$$

CH_4 selectivity and CO selectivity were calculated as the following:

$$CH_4 \text{ selectivity } (\%) = \frac{CH_{4\ \text{outlet}}}{CO_{2\ \text{inlet}} - CO_{2\ \text{outlet}}} \times 100\%$$

$$CO \text{ selectivity } (\%) = \frac{CO_{\ \text{outlet}}}{CO_{2\ \text{inlet}} - CO_{2\ \text{outlet}}} \times 100\%$$

Where $CO_{2\ \text{inlet}}$ and $CO_{2\ \text{outlet}}$ represent the CO_2 concentration in the feed and effluent, respectively, and $CH_{4\ \text{outlet}}$ and CO_{outlet} represent the concentration of CH_4 and CO in the effluent, respectively.

3. Results and discussion

3.1. In situ XPS

XPS was performed for both pretreated and spent catalysts to determine the chemical state and the relative proportion of elements on the surface. High resolution Ce 3d spectrum regions were fit with the method described by Eric Beche et al. thus four peaks represent the Ce^{3+} oxidation state and six peaks represent the Ce^{4+} oxidation state (Bêche et al., 2008). The conventional peak labels suggested by Burroughs et al. were used to denote components of the Ce 3d region, where v and u denote the 5/2 and 3/2 doublet components respectively (Burroughs et al., 1976). We also collected spectra of the synthesized pure CeO_2 where the Ce^{3+}/Ce^{4+} ratio had been proved to be ∼0.11, which is in accordance with the literature (Varga et al., 2015). Collected and fit spectra are presented in the Supplementary Information (Fig. S9, S10).

Fig. S9 compares the Ce 3d spectra of 4 mol% NiO/CeO_2 and $Ce_{0.96}Ni_{0.04}O_2$ catalysts after pretreatment and after reaction. Comparing the observed 3d envelope with those previously reported for Ce^{4+} and Ce^{3+} indicates that both the pretreated and spent catalysts contain mixed valence states of Ce^{4+} and Ce^{3+} ions (Ferencz et al., 2014; Óvári et al., 2013). The percentages of Ce^{3+} and Ce^{4+} ions were calculated based on the integrated peak areas as shown in Table 1. The Ce^{3+}/Ce^{4+} ratio is higher on the 4 mol% NiO/CeO_2 spent catalyst than that on the other catalysts. This indicates higher OSC, which favors high CO_2 conversion and CO_2 consumption rate.

The low concentration of Ni present in the samples made the detection a serious challenge. (Because of the overlap of Ni 2p 1/2 and Ce 3d 3/2 peaks and lower Scofield RSF value of Ni compared to Ce.) To acquire data about Ni only the Ni 2p 3/2 spectrum region was fit. Two peaks were distinguished during the procedure, a metallic Ni^0 peak at ∼852.6 eV, which was fit with an asymmetric peak shape (Biesinger et al., 2011) and an oxide peak at ∼855.4 eV. This binding energy is higher than the binding energy observed for pure NiO (∼853.4 eV) (Lian et al., 1992) and is characteristic of oxide structures where another metal is present beside Ni^{2+} ions (McIntyre and Cook, 1975). The ratio of Ni^0/Ni^{2+} species is presented in Table 1. In the case of the 4 mol% NiO/CeO_2 sample, Ni is mostly present as Ni^0, which serves as an active site for H_2 spillover, promoting CH_4 production. The Ce^{3+}/Ce^{4+} of $Ce_{0.96}Ni_{0.04}O_2$ decreases from pretreatment to reaction, indicating that Ce^{3+} and Ni^{2+} are competing for the reduction, thus slowing down the reduction of Ni^{2+} species.

3.2. HAADF and EDX

According to the HAADF and EDX imaging (Fig. 1) of the catalysts, after reduction the dispersion of Ni is more homogeneous in the $Ce_{0.96}Ni_{0.04}O_2$ sample, which is accounted for the formation of nanoclusters. It is hard to determine their exact size due to the homogeneity, according to the image the particles have ∼5 nm diameter. Also, it is important to note that single-atom catalysis is ruled out since those are usually created with less than 0.05 wt% of the supported material (DeRita et al., 2017). In the 4 mol% NiO/CeO_2 sample locally grouped Ni atoms are observed, creating separated inclusions in the form of nanoparticles, which have ∼10 nm diameter.

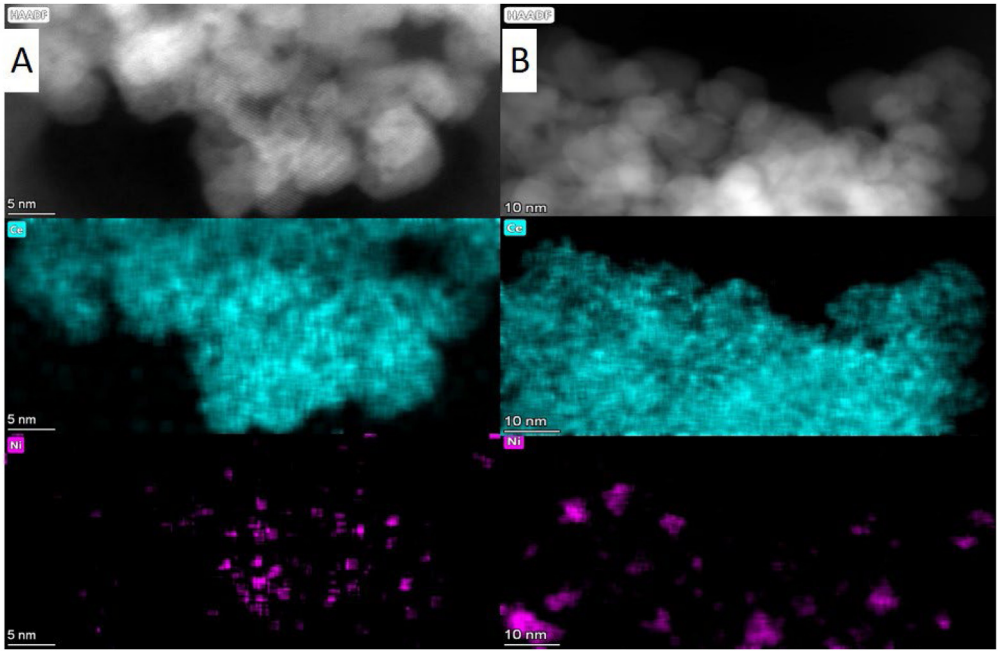

Fig. 1. 1. HAADF and EDX images of the (A) solid solution and (B) impregnated catalysts after pretreatment at 300 °C.

3.3. Catalytic performance

Catalytic performance of the prepared samples was tested in CO_2 hydrogenation reaction. Fig. 2 displays the CO_2 consumption rate as a function of reaction temperature for the catalysts. CO_2 conversion and selectivity of the catalysts are summarized in Table 2. Pure CeO_2 favors the formation of methanol and ethanol at low temperatures. Modification by Ni species suppressed the formation of alcohols. When the pre-reduction temperature was 300 °C the CO_2 conversion for 4 mol% NiO/CeO_2 was 65% (CH_4 selectivity = 94.71% at 400 °C) at 400 °C which is 10 times higher than the $Ce_{0.96}Ni_{0.04}O_2$ solid solution catalyst which had a CO_2 conversion of 6.39% (CH_4 selectivity = 4.48% at 400 °C). This indicates that NiO present on the surface of CeO_2 is more active than Ni^{2+} ions in the lattice. CH_4 was formed as the major product and CO as a minor product on the interfacial catalyst (4 mol% NiO/CeO_2 catalysts) while CO was formed as the major product and CH_4 as a minor product on the $Ce_{0.96}Ni_{0.04}O_2$ solid solution catalyst. This indicated that Ni present on the surface of CeO_2 produces selectively CH_4 due to the stronger hydrogenation ability of Ni. However, Ni present in the solid solution does not expose during the hydrogenation reaction, hence does not contribute to the CH_4 formation. It is observed that CO_2 conversion was zero at low temperatures over the $Ce_{0.96}Ni_{0.04}O_2$ solid solution catalyst and improved at higher temperatures. This could be attributed to the absence of potential active surface sites for the CO_2 adsorption on the $Ce_{0.96}Ni_{0.04}O_2$ solid solution catalyst. In addition, *in situ* XPS analysis of the spent catalysts revealed that the Ce^{3+}/Ce^{4+} ratio in 4 mol% NiO/CeO_2 was 0.37 compared to the value of 0.18 in $Ce_{0.96}Ni_{0.04}O_2$ solid solution catalyst (Table 1.), which is marginally higher than the value of 0.11 characteristic to pure CeO_2. The high Ce^{3+}/Ce^{4+} ratio over 4 mol% NiO/CeO_2 boosted its CO_2 conversion and consumption rate. It is important to note that a lower BET surface area (Table S1 of the Supplementary Information) was obtained for 4 mol% NiO/CeO_2 (86.12 m^2g^{-1}) compared to $Ce_{0.96}Ni_{0.04}O_2$ (123.18 m^2g^{-1}), implying that the impact of the specific surface area is a lesser contributing factor to CO_2 conversion.

The catalytic performance is further investigated based on the CO_2 consumption rate of the catalysts during reaction. It is important to note, that according to the *in situ* XPS results, no Ni^0 is forming in the $Ce_{0.96}Ni_{0.04}O_2$ solid solution catalyst until the reaction temperature passes 300 °C. Fig. 2 illustrates the impact of the reduction of Ni^{2+} to Ni^0 between 300 °C and 400 °C, significantly increasing the consumption rate of the $Ce_{0.96}Ni_{0.04}O_2$ catalyst.

Also at this temperature we achieve the highest CO_2 consumption rate (31.82 μmol/gs) with the 4 mol% NiO/CeO_2 sample. In comparison, the $Ce_{0.96}Ni_{0.04}O_2$ solid solution counterpart has CO_2 consumption rate of 0.87 μmol/gs at 400 °C. To further emphasize the importance of Ni^0 species and the interface it creates with the Ce_{2-x} we calculated the CO_2 consumption rate specific to surface Ni^0 species (Fig. 4) which proves to be 2.7 times higher for 4 mol% NiO/CeO_2 compared to $Ce_{0.96}Ni_{0.04}O_2$.

In the case of reactions with 600 °C pre-reduction, both catalysts exhibit similar activity, as is shown in Fig. 3B. This is mainly due to the high pre-reduction temperature, where hydrogen could successfully reduce the catalysts, creating lattice defects and allowing a significant increase in the reduction of Ni^{2+} species. *Ex situ* XPS measurements (Fig. S11, Table S7) of the spent samples confirm, that 67% and 51% of Ni is present as Ni^0 in $Ce_{0.96}Ni_{0.04}O_2$ and 4 mol% NiO/CeO_2,

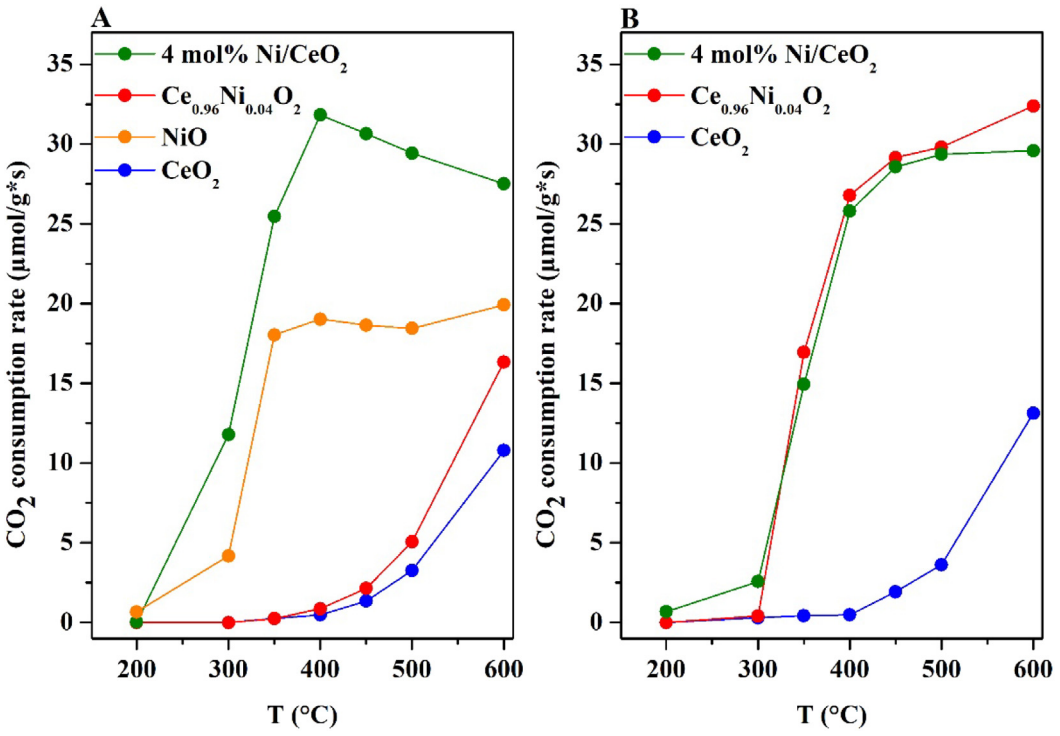

Fig. 2. CO_2 consumption rate as a function of temperature over CeO_2, $Ce_{0.96}Ni_{0.04}O_2$ solid solution, and 4 mol% NiO impregnated CeO_2 and NiO catalysts. (A) Pre-reduced in H_2 at 300 °C (B) Pre-reduced in H_2 at 600 °C.

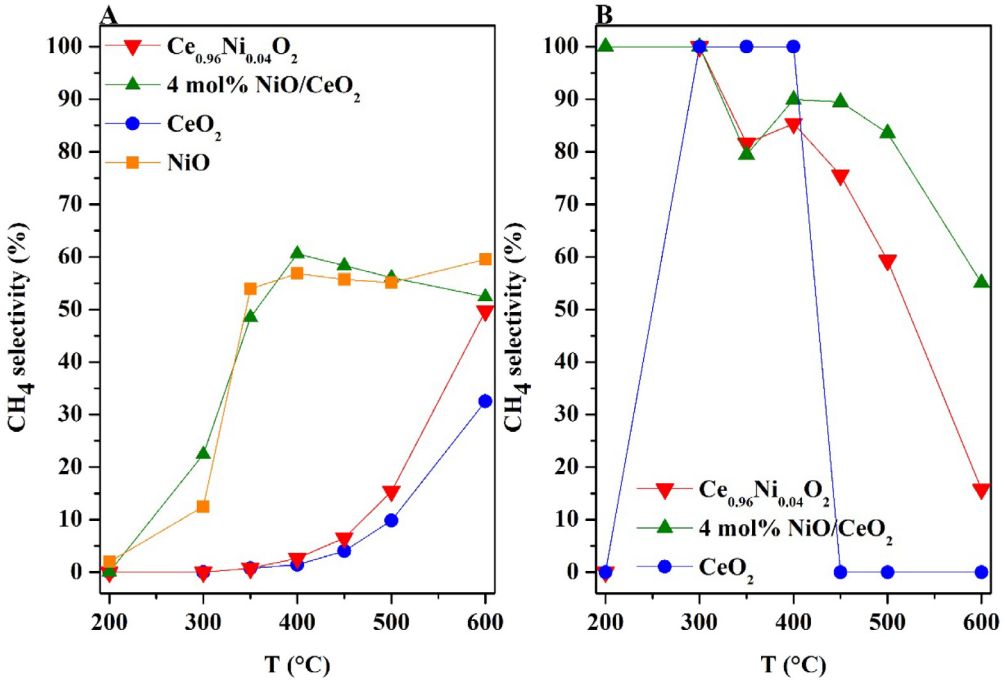

Fig. 3. Methane selectivity of the investigated catalysts, with different pretreatment temperatures. (A) Pre-reduced in H_2 at 300 °C (B) Pre-reduced in H_2 at 600 °C.

respectively. As for selectivity, a significant decrease is observed in methane selectivity after 400 °C. This is accounted for the formation of CO being the thermodynamically favored process instead of the formation of CH_4.

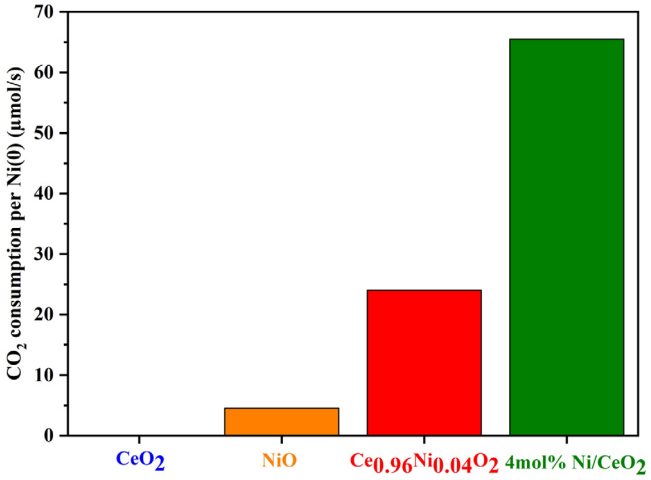

Fig. 4. CO_2 consumption rates calculated as a function of available Ni^0 species on the surface at 400 °C.

Table 2
Conversion and selectivity for CO_2 hydrogenation over various catalysts.[a]

Catalysts	CO_2 Conversion (%)	Selectivity (%)		
		CO	CH_4	C_2H_6
CeO_2	9.92	100	0	0
$Ce_{0.96}Ni_{0.04}O_2$	6.39	95.52	4.48	0
4 mol% NiO/CeO_2	65.16	5.29	94.71	0
NiO	67.86	8.14	91.86	0

[a]Reaction conditions: T = 400 °C, CO_2/H_2 = 1/4, catalyst weight = 0.15 g.

3.4. Operando DRIFTS study

To identify the possible reaction intermediates and the composition of the gas phase in the CO_2 hydrogenation reaction, *operando* DRIFTS measurements were performed under reaction conditions. The *operando* DRIFT spectra were recorded from 50 °C to 400 °C for CeO_2 (Fig. S12), 4 mol% NiO/CeO_2, and $Ce_{0.96}Ni_{0.04}O_2$ catalysts pretreated at different temperatures (Fig. 5). The types of intermediate species and their corresponding DRIFT vibrational frequencies obtained on pure CeO_2, modified CeO_2, and NiO are summarized in the Supplementary Information (Table S7.)

It is generally observed in CO_2 hydrogenation reactions that the activated CO_2 (CO_2^*) forms (vibrationally or electronically) in the first step (Cheng and Lo, 2016; Freund and Roberts, 1996; Sápi et al., 2018). In the case of ceria based catalysts, the most important active sites for CO_2 activation are the lattice defects (Ce^{3+}). which is proven by experimental data and density functional theory calculation combining microkinetic analysis (Cheng and Lo, 2016). The activated CO_2 species transform further in different ways according to the nature and oxidation state of modifiers. CeO_2 performs complex DRIFT spectral features. Its comprehensive analysis is important to draw a conclusion from the IR spectra obtained on Ni enhanced ceria. The DRIFT spectra obtained during CO_2 hydrogenation on unmodified CeO_2 are displayed in Fig. S12 A and the detailed analysis and conclusion are discussed in Supplementary Information. Only the main results, which are important for understanding the characteristic feature of the reaction, are summarized in this paragraph. The overtones of gas-phase CO_2 and OH bond modes appeared between 3600 and 3727 cm^{-1}. The activated bent $CO_2^{\delta-}$ formed on vacancy sites reacts with OH groups giving bicarbonate or carboxylate species (Collins et al., 2006). Peaks at ~1650 cm^{-1} and 1287 cm^{-1} can be assigned to $\nu_3(O–C–O)_a$ and $\nu_3(O–C–O)_s$ respectively of carboxylate (CO_2^-) vibrational modes (Baltrusaitis et al., 2011; Su et al., 2008).

The bands centered at ~1614, ~1370, 1212 cm^{-1} can be assigned to the $\nu_2(O\text{-}C\text{-}O)_a$, $\nu_3(O\text{-}C\text{-}O)_s$, and $\delta_4(C\text{-}OH)$ vibration modes respectively which were ascribed to the bicarbonate species (Fig. 12SA) (Sápi et al., 2018). The bicarbonate and carboxylate could convert to formate species, which play an important role in CO_2 hydrogenation on ceria based catalysts. Several different carbonates are also formed during the CO_2 adsorption and its hydrogenation, which do not participate in the process on CeO_2. Bridge bonded carbonates (two or three oxygen bonds to ceria surface) and bridge bonded hydrogen carbonate appear in a broad range at ~1212–1232 cm^{-1} (Vayssilov et al., 2011) They are present even at 400 °C with high intensity. This very stable carbonate may be inactive in the CO_2 hydrogenation and it could contribute to the inhibition of the reaction. The characteristic vibrations (symmetric and asymmetric O-C-O and C-H modes) of formate appeared at 1560–1600, 1350–1380, and 2837 cm^{-1} (Guo et al., 2018; Lin et al., 2018; Raskó et al., 2004; Wang et al., 2016). On pure

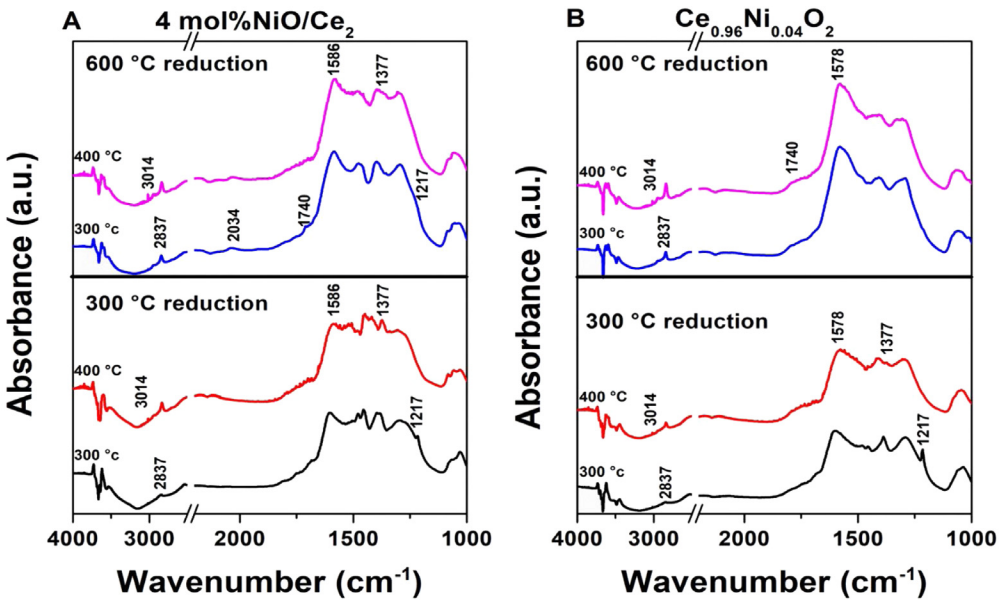

Fig. 5. DRIFTS spectra of (A) 4 mol% NiO/CeO_2 and (B) $Ce_{0.96}Ni_{0.04}O_2$ obtained during CO_2 hydrogenation after different pre-reduction temperatures.

NiO, the IR bands obtained during CO_2 hydrogenation are identical to the published data earlier (Sápi et al., 2018) and are listed in Table S6.

Ni enhanced CeO_2 catalysts and their DRIFT spectra have different features during CO_2 hydrogenation. The dominant intermediate is the bicarbonate on both impregnated and solid solution samples at a low temperature range. The main IR bands for bicarbonate were detected at 1602–1611, 1408–1430, and 1216 cm^{-1} (Table S6). These peaks disappeared around 250–350 °C. The peak around 1280–1292 cm^{-1} is attributable to bidentate carbonate (Baltrusaitis et al., 2011; Guo et al., 2018; Lee et al., 2019). We should note that the very stable bridge bonded carbonates (at ∼1212–1232 cm^{-1}) could not be detected on Ni enhanced CeO_2 catalysts. The important bands for formate are visible at ∼1574-1585, 1398–1374, and 2837–2844 cm^{-1} above 200 °C (Fig. 5 A and B). It should be mentioned that formate was found also as a key intermediate during CO_2 methanation on Ni containing ceria catalyst prepared with simple impregnation or with a modified hydrothermal method, published recently (Yu et al., 2021). In addition, Lee et al. (2019) presumed that, besides formate, a monodentate carbonate could be another intermediate in methane formation, especially at higher temperatures. In our case, this species is detected at 1387–1395 cm^{-1}.

Fig. 5A and B present the most important information about the reaction intermediates formed during CO_2 hydrogenation on the impregnated NiO/CeO_2 and the $Ce_{0.96}Ni_{0.04}O_2$ catalysts after different pre-treatments (300 °C and 600 °C). It is demonstrated in the figures, that the pre-reduction temperatures influence the amount and the thermal stability of formate. The results are compared at the same (∼4%) Ni content. The figures present some selected spectra obtained at 300 and 400 °C.

Based on the literature and our data, we may conclude that the formate species originate from bicarbonate species. Bicarbonate disappeared when the formate bands showed up:

$$CO_{2(a)}{}^{*} + H_{(a)}(OH_{(a)}) \rightarrow HCO_3^- \quad (1)$$

$$HCO_{3\,(ads)}^- + H_{(ads)} \rightarrow HCOO_{(ads)}^- + OH_{(ads)} \quad (2)$$

The further reaction of formate species likely determines the final products, and the type of modifiers may alter the reaction routes of formate. On pure ceria the formate decomposition only produced CO above 300 °C. A similar reaction mechanism was suggested for other similar catalytic systems (László et al., 2019; Sápi et al., 2018; Wang et al., 2017; Zhao et al., 2019).

$$HCOO_{(a)} \rightarrow CO_{(a)} + OH_{(a)} \rightarrow CO_{(g)} + H_2O_{(g)} \quad (3)$$

CO formation in CO_2 hydrogenation can be also be explained via carboxylate (COOH) intermediate as it was suggested previously on clean ceria catalysts, too (Cheng and Lo, 2016):

$$COOH^{*}{}_{(a)} \rightarrow CO^{*}{}_{(a)} + OH_{(a)} \rightarrow CO_{(g)} + H_2O_{(g)} \quad (4)$$

These reaction sequences could be valid for the explanation of CO production in both types of Ni containing catalysts to a certain extent.

In Fig. 5 A at 300 °C pre-reduction the intensity of bicarbonate (1216 cm^{-1}) drastically decreased at 300 °C, and at the same time formate bands are developed (2844, ~1585–1590, and 1377 cm^{-1}). By increasing the temperature, the intensity of formate increased and the bands for gas phase methane and CO also intensified. At these temperatures, polydentate (1447 cm^{-1}) and monodentate (1508 cm^{-1}) carbonates are also present. Some features between 1100 and 900 cm^{-1} may correspond to these carbonate-like species.

The catalytic measurements strongly indicate that the methane is formed with high selectivity on mixed oxides. XPS experiments revealed that metallic particles are produced and the Ce^{3+} concentration notably increased by hydrogen pre-treatment. The high methane selectivity on Ni modified ceria catalysts can be explained by the Ni^0 particle assisted reaction between formate and hydrogen. The main role of Ni^0 and support CeO_2 were to dissociate H_2. This conclusion was also drawn in similar Ni^0 containing systems (Cheng and Lo, 2016; Yu et al., 2021). The reduced Ni particles help to produce the high amount of hydrogen needed to convert formates, which are located mainly at the Ni-ceria interface (Ni^0 – NiO – CeO_2):

$$HCOO_{(a)} + 2H_{(a)} \rightarrow H_2CO_{(a)} \rightarrow H_2C_{(a)} + OH_{(a)} \quad (5)$$

$$H_2C_{(a)} + 2H_{(a)} \rightarrow CH_{4(g)} \quad (6)$$

When hydrogen pretreatment was carried out at 600 °C, we obtained qualitatively the same picture (Fig. 5 A). Some differences can be attributed to the increased amount of metallic Ni, since Pre-reduction at 600 °C results in higher Ni^0 concentration. Consequently, we detected a higher methane yield. The other remarkable difference is that the formate appeared at a lower temperature (200 °C) and in higher concentration at 300–400 °C than it was observed after 300 °C reduction (Fig. 5 A). The bicarbonate bands disappeared at lower temperatures (200 °C) in this case. This means that metallic Ni could catalyze not only the formate-hydrogen reaction but helps the bicarbonate-formate transformation, too (step 2).

After careful analysis of the spectra obtained during the reaction, a very weak band for adsorbed CO at ~2034 cm^{-1} was detectable. Its intensity was much higher when a higher number of Ni^0 particles are present (Fig. 5 A at 600 °C reduction). Adsorbed CO formation was also detected on almost similar systems previously (Lee et al., 2019; Yu et al., 2021). The origin of adsorbed CO can be attributed to the decomposition of formate or carboxylate (steps 3, 4). The other realistic scenario for adsorbed (or gas phase) CO formation is the transformation of formate to formaldehyde-like species, H_2CO. This species may decompose to CO at elevated temperatures. Indeed, our spectra show a weak band at 1740 cm^{-1} above 350 °C. This band can be tentatively attributed to formaldehyde or formyl-like species, also derived from formate, which was reported on Ru/CeO_2 and NiO catalysts during the CO_2 hydrogenation (Sápi et al., 2018; Wang et al., 2016). The formation and decomposition of formyl to CO could alter the methane selectivity in CO_2 hydrogenation.

Formaldehyde formation in HCOOH decomposition was observed previously on Pt supported TiO_2 (Raskó et al., 2004), and the formation and decomposition of formaldehyde on TiO_2 supported Rh and Au catalysts were studied earlier (Kecskés et al., 2004).

$$CH_2O^*_{(a)} \rightarrow CO_{(g)} + OH_{(a)} \quad (7)$$

The CO_2 hydrogenation was also followed by DRIFTS on the solid solution sample at the same Ni quantity pre-reduced at two temperatures (Fig. 5B). The bicarbonate species were present up to 300–350 °C when the catalyst was pre-reduced at 300 °C. When the bicarbonate diminished, the formate showed up. From 300 °C its intensity increased continuously. The reaction proceeds with low conversion and high CO selectivity. In this case, the significant amount of formate decomposes via step 3, where the product is mainly CO. A new band was also developed at 1740 cm^{-1} above 350 °C due to the formation of formyl-like species, which decomposes also to CO as it was discussed in previous cases (steps 5, 7).

When the catalyst was pre-reduced at 600 °C, more metallic Ni is formed, and the conversion of the reaction increased with high methane selectivity. The bicarbonate band disappeared already at 200 °C and the formate appeared at 200 °C, its intensity increased up to 350–400 °C (Fig. 5B). In these circumstances, the methane formation proceeds mainly via hydrogenation of formate. These results underline the importance of the role of Ni^0 in the CO_2 methanation. It is turned out again that the metallic Ni catalysis first the bicarbonate-formate transformation (step 2) and then the hydrogenation of formate to methane (step 5,6). The catalytic measurements showed that the activities of impregnated and mixed oxide catalysts perform nearly the same activity and selectivity if the pre-reduction happens at 600 °C. Conversely, the TEM results indicate that the particle sizes are somewhat different (2–3 nm in the mixed oxide and ~5 nm in the impregnated sample) despite this fact the activities do not differ significantly. These experimental data suggest that the size effect does not play a decisive factor in this range. The most important factor is the Ni^0/NiO ratio in the Ni^0-NiO-CeO_x interface.

4. Conclusions and summary

Ni/NiO enhanced CeO_2 based catalysts were tested in CO_2 hydrogenation with the objective to demonstrate the importance of metallic Ni and Ni^0-NiO-CeO_{2-x} interface. Two catalysts, a NiO-CeO_2 solid solution (labeled as $Ce_{0.96}Ni_{0.04}O_2$) and CeO_2 supported NiO nanoparticles, impregnated catalysts (labeled as 4 mol% NiO/CeO_2) were prepared. Differing from solid solutions, the catalytic behavior of impregnated catalyst retaining an interface was significantly better regarding conversion and product selectivity due to the formation of Ni^0-NiO-CeO_{2-x}, the hydrogen spillover phenomena, and the

more reduced state of the CeO_2. The metallic Ni content was tunable by the temperature of hydrogen pretreatment. The impregnated catalyst with significant metallic content exhibited high activity and high methane selectivity. The mixed oxide was more resistant to reduction, in the case of both the Ni^{2+} and Ce^{4+} species. This type of catalyst has low activity with high CO selectivity. The activity and methane selectivity increased considerably by increasing the metal content or higher hydrogen pretreatment temperature. The 4 mol% NiO/CeO_2 catalyst showed a CO_2 conversion of 65% with the methane selectivity of 95% at 400 °C which is 10 times higher compared to the $Ce_{0.96}Ni_{0.04}O_2$ solid solution counterpart (CO_2 conversion = 6.39%, CO selectivity = 95% at 400 °C), indicating that $Ni/NiO/CeO_2$ interfacial catalyst is more active than the solid solution where the Ni^{2+} ions are built into the crystal lattice. XPS showed that the Ce^{3+}/Ce^{4+} ratio is higher on the 4 mol% NiO/CeO_2 spent catalyst than that on the other catalysts. The reason for the higher activity of the interfacial sample is the synergistic effect of the higher Ni^0 concentration on the sample surface (also confirmed by XPS), the reducibility of the CeO_2 support, which provides catalytically active sites for the $O = C = O$ bonds to be broken, facilitating the conversion to methane. Ni^0 supplies a significant amount of hydrogen atoms, which react with formate intermediates located at the Ni^0-NiO-CeO_{2-x} interface. The critical concentration of metallic Ni helps to create the proper interface, which also plays an important role in methanation. In the case of the $Ce_{0.96}Ni_{0.04}O_2$ counterpart, the Ni distribution is rather uniform, supposing a lower particle size than the impregnated sample (confirmed by HAADF STEM), therefore the proper interface did not develop after 300 °C reduction. High temperature reduction (∼600 °C) is necessary to reach the same active interface in these types of catalysts. *Operando* DRIFT spectral results show that the bicarbonate species is the origin of formate surface intermediates, which play important role in methane formation. It is concluded that metallic Ni catalyzes not only the methane production from formate but also the bicarbonate-formate transformation. The most important factor in the high performance of the catalysts is the Ni^0/NiO ratio in the Ni^0-NiO-CeO_x interface.

CRediT authorship contribution statement

Ákos Szamosvölgyi: Conception and design of study, Writing – original draft. **T. Rajkumar:** Conception and design of study. **András Sápi:** Conception and design of study, Writing – original draft. **Imre Szenti:** Analysis and/or interpretation of data. **Marietta Ábel:** Analysis and/or interpretation of data. **Juan Fernando Gómez-Pérez:** Writing – review & editing. **Kornélia Baán:** Acquisition of data. **Zsolt Fogarassy:** Acquisition of data. **Erzsébet Dodony:** Acquisition of data. **Béla Pécz:** Writing – original draft. **Seema Garg:** Analysis and/or interpretation of data. **János Kiss:** Acquisition of data, Writing – review & editing. **Ákos Kukovecz:** Writing – original draft. **Zoltán Kónya:** Writing – original draft.

Declaration of competing interest

The authors declare that they have no known competing financial interests or personal relationships that could have appeared to influence the work reported in this paper.

Acknowledgments

Project no. TKP2021-NVA-19 has been implemented with the support provided by the Ministry of Innovation and Technology of Hungary from the National Research, Development, and Innovation Fund, financed under the TKP2021-NVA funding scheme. AS gratefully acknowledges the support of the Bolyai Janos Research Fellowship of the Hungarian Academy of Science and the "UNKP-21-5-SZTE-586" New National Excellence Program as well as the funding provided by the Indo-Hungarian TÉT project (2019-2.1.13-TÉT_IN-2020-00015) of the Ministry for Innovation and Technology from the source of the National Research, Development and Innovation. ISZ is grateful for the fund of the "UNKP-21-4-SZTE-533" New National Excellence Program of the Ministry for Innovation and Technology. KZ is grateful for the fund of NKFIH - OTKA - SNN 135918 and K_21 138714. The financial support of the Hungarian National Research, Development, and Innovation Office through the GINOP-2.3.2-15-2016-00013 project "Intelligent materials based on functional surfaces - from syntheses to applications" and the Ministry of Human Capacities through the EFOP-3.6.1-16-2016-00014 project and the 20391-3/2018/FEKUSTRAT are acknowledged. Access to the STEM microscope facility is provided via the VEKOP-2.3.3-15-2016-00002 project of the European Structural and Investment Funds. All authors approved the version of the manuscript to be published.

Appendix A. Supplementary data

Supplementary material related to this article can be found online at https://doi.org/10.1016/j.eti.2022.102747.

References

Baltrusaitis, J., Schuttlefield, J., Zeitler, E., Grassian, V.H., 2011. Carbon dioxide adsorption on oxide nanoparticle surfaces. Chem. Eng. J. 170 (2), 471–481.

Bêche, E., Charvin, P., Perarnau, D., Abanades, S., Flamant, G., 2008. Ce 3d XPS investigation of cerium oxides and mixed cerium oxide (CexTiyOz). Surf. Interface Anal. 40 (3–4), 264–267.

Biesinger, M.C., Payne, B.P., Grosvenor, A.P., Lau, L.W.M., Gerson, A.R., Smart, R.S.C., 2011. Resolving surface chemical states in XPS analysis of first row transition metals, oxides and hydroxides: Cr, Mn, Fe, Co and Ni. Appl. Surf. Sci. 257 (7), 2717–2730.

Burroughs, P., Hamnett, A., Orchard, A.F., Thornton, G., 1976. Satellite structure in the X-ray photoelectron spectra of some binary and mixed oxides of lanthanum and cerium. J. Chem. Soc. Dalton Trans.(17) 1686–1698.

Centi, G., Quadrelli, E.A., Perathoner, S., 2013. Catalysis for CO 2 conversion: a key technology for rapid introduction of renewable energy in the value chain of chemical industries. Energy Environ. Sci. 6 (6), 1711–1731.

Cheng, Z., Lo, C.S., 2016. Mechanistic and microkinetic analysis of CO2 hydrogenation on ceria. Phys. Chem. Chem. Phys. 18 (11), 7987–7996.

Collins, S.E., Baltanás, M.A., Bonivardi, A.L., 2006. Infrared spectroscopic study of the carbon dioxide adsorption on the surface of Ga2O3 polymorphs. J. Phys. Chem. B 110 (11), 5498–5507.

Daza, Y.A., Kuhn, J.N., 2016. CO 2 conversion by reverse water gas shift catalysis: comparison of catalysts, mechanisms and their consequences for CO 2 conversion to liquid fuels. RSC Adv. 6 (55), 49675–49691.

DeRita, L., Dai, S., Lopez-Zepeda, K., Pham, N., Graham, G.W., Pan, X., Christopher, P., 2017. Catalyst architecture for stable single atom dispersion enables site-specific spectroscopic and reactivity measurements of CO adsorbed to Pt atoms, oxidized Pt clusters, and metallic Pt clusters on TiO2. J. Am. Chem. Soc. 139 (40), 14150–14165.

Ferencz, Z., Erdőhelyi, A., Baán, K., Oszkó, A., Óvári, L., Kónya, Z., Papp, C., Steinrück, H.P., Kiss, J., 2014. Effects of support and Rh additive on co-based catalysts in the ethanol steam reforming reaction. ACS Catal. 4 (4), 1205–1218.

Freund, H.-J., Roberts, M.W., 1996. Surface chemistry of carbon dioxide. Surf. Sci. Rep. 25 (8), 225–273.

Frontera, P., Macario, A., Ferraro, M., Antonucci, P., 2017. Supported catalysts for CO2 methanation: a review. Catalysts 7 (2), 59.

Guo, Y., Mei, S., Yuan, K., Wang, D.-J., Liu, H.-C., Yan, C.-H., Zhang, Y.-W., 2018. Low-temperature CO2 methanation over CeO2-supported Ru single atoms, nanoclusters, and nanoparticles competitively tuned by strong metal–support interactions and H-spillover effect. ACS Catal. 8 (7), 6203–6215.

Kecskés, T., Raskó, J., Kiss, J., 2004. FTIR And mass spectrometric study of HCOOH interaction with TiO2 supported Rh and Au catalysts. Appl. Catal. A: General 268 (1), 9–16.

Kiss, J., Kukovecz, Á., Kónya, Z., 2019. Beyond nanoparticles: the role of sub-nanosized metal species in heterogeneous catalysis. Catal. Lett. 149 (6), 1441–1454.

László, B., Baán, K., Ferencz, Z., Galbács, G., Oszkó, A., Kónya, Z., Kiss, J., Erdőohelyi, A., 2019. Gold size effect in the thermal-induced reaction of CO2 and H2 on Titania- and Titanate nanotube-supported gold catalysts. J. Nanosci. Nanotechnol. 19 (1), 470–477.

Lee, S.M., Lee, Y.H., Moon, D.H., Ahn, J.Y., Nguyen, D.D., Chang, S.W., Kim, S.S., 2019. Reaction mechanism and catalytic impact of Ni/CeO2–x catalyst for low-temperature CO2 methanation. Ind. Eng. Chem. Res. 58 (20), 8656–8662.

Li, H., Li, K., Wang, H., Zhu, X., Wei, Y., Yan, D., Cheng, X., Zhai, K., 2016. Soot combustion over Ce1-xFexO2-δ and CeO2/Fe2O3 catalysts: Roles of solid solution and interfacial interactions in the mixed oxides. Appl. Surf. Sci. 390, 513–525.

Lian, K., Thorpe, S.J., Kirk, D.W., 1992. Electrochemical and surface characterization of electrocatalytically active amorphous Ni · Co alloys. Electrochim. Acta 37 (11), 2029–2041.

Lin, L., Yao, S., Liu, Z., Zhang, F., Li, N., Vovchok, D., Martínez-Arias, A., Castañeda, R., Lin, J., Senanayake, S.D., 2018. In situ characterization of cu/CeO2 nanocatalysts for CO2 hydrogenation: Morphological effects of nanostructured ceria on the catalytic activity. J. Phys. Chem. C 122 (24), 12934–12943.

Luk, H.T., Mondelli, C., Ferré, .D.C., Stewart, J.A., Pérez-Ramírez, J., 2017. Status and prospects in higher alcohols synthesis from syngas. Chem. Soc. Rev. 46 (5), 1358–1426.

Maitarad, P., Han, J., Zhang, D., Shi, L., Namuangruk, S., Rungrotmongkol, T., 2014. Structure–activity relationships of NiO on CeO2 nanorods for the selective catalytic reduction of NO with NH3: experimental and DFT studies. J. Phys. Chem. C 118 (18), 9612–9620.

McIntyre, N.S., Cook, M.G., 1975. X-ray photoelectron studies on some oxides and hydroxides of cobalt, nickel, and copper. Anal. Chem. 47 (13), 2208–2213.

Montini, T., Melchionna, M., Monai, M., Fornasiero, P., 2016. Fundamentals and catalytic applications of CeO2-based materials. Chem. Rev. 116 (10), 5987–6041.

Óvári, L., Calderon, S.Krick., Lykhach, Y., Libuda, J., Erdőhelyi, A., Papp, C., Kiss, J., Steinrück, H.P., 2013. Near ambient pressure XPS investigation of the interaction of ethanol with Co/Ceo2(111). J. Catal. 307, 132–139.

Porosoff, M.D., Yan, B., Chen, J.G., 2016. Catalytic reduction of CO 2 by H 2 for synthesis of CO, methanol and hydrocarbons: challenges and opportunities. Energy Environ. Sci. 9 (1), 62–73.

Rajkumar, T., Sápi, A., Ábel, M., Kiss, J., Szenti, I., Baán, K., Gómez-Pérez, J.F., Kukovecz, Á., Kónya, Z., 2021. Surface engineering of CeO2 catalysts: Differences between solid solution based and interfacially designed Ce1-xMxO2 and MO/CeO2 (M = Zn, Mn) in CO2 hydrogenation reaction. Catal. Lett. 151, 3477–3491.

Raskó, J., Kecskés, T., Kiss, J., 2004. Formaldehyde formation in the interaction of HCOOH with Pt supported on TiO2. J. Catal. 224 (2), 261–268.

Sápi, A., Halasi, G., Kiss, J., Dobó, .D.G., Juhász, K.L., Kolcsár, V.J., Ferencz, Z., Vári, G., Matolin, V., Erdőhelyi, A., Kukovecz, Á, Kónya, Z., 2018. In situ DRIFTS and NAP-XPS exploration of the complexity of CO2 hydrogenation over size-controlled Pt nanoparticles supported on mesoporous NiO. J. Phys. Chem. C 122 (10), 5553–5565.

Sápi, A., Kashaboina, U., Ábrahámné, .K.B., Gomez, J.P., Szenti, I., Halasi, G., Kiss, J., Nagy, B., Varga, T., Kukovecz, Á., 2019a. Synergetic of pt nanoparticles and H-ZSM-5 zeolites for efficient CO2 activation: Role of interfacial sites in high activity. Front. Mater. 6, 127.

Sápi, A., Rajkumar, T., Ábel, M., Efremova, A., Grósz, A., Gyuris, A., Ábrahámné, .K.B., Szenti, I., Kiss, J., Varga, T., 2019b. Noble-metal-free and pt nanoparticles-loaded, mesoporous oxides as efficient catalysts for CO2 hydrogenation and dry reforming with methane. J. CO2 Util. 32, 106–118.

Selvamani, A., Selvaraj, M., Krishnan, P.S., Gurulakshmi, M., Shanthi, K., 2015. Low temperature vapor phase selective oxidation of ethylbenzene over Ce1- xMnxO2 nanocubes. Appl. Catal A: General 495, 92–103.

Su, W., Zhang, J., Feng, Z., Chen, T., Ying, P., Li, C., 2008. Surface phases of TiO2 nanoparticles studied by UV Raman spectroscopy and FT-ir spectroscopy. J. Phys. Chem. C 112 (20), 7710–7716.

Varga, E., Ferencz, Z., Oszkó, A., Erdőhelyi, A., Kiss, J., 2015. Oxidation states of active catalytic centers in ethanol steam reforming reaction on ceria based rh promoted co catalysts: An XPS study. J. Mol. Catal. A: Chemical 397, 127–133.

Vayssilov, G.N., Mihaylov, M., Petkov, P.S., Hadjiivanov, K.I., Neyman, K.M., 2011. Reassignment of the vibrational spectra of carbonates, formates, and related surface species on ceria: A combined density functional and infrared spectroscopy investigation. J. Phys. Chem. C 115 (47), 23435–23454.

Vogt, C., Groeneveld, E., Kamsma, G., Nachtegaal, M., Lu, L., Kiely, C.J., Berben, P.H., Meirer, F., Weckhuysen, B.M., 2018. Unravelling structure sensitivity in CO 2 hydrogenation over nickel. Nat. Catal. 1 (2), 127–134.
Wang, F., He, S., Chen, H., Wang, B., Zheng, L., Wei, M., Evans, D.G., Duan, X., 2016. Active site dependent reaction mechanism over ru/CeO2 catalyst toward CO2 methanation. J. Am. Chem. Soc. 138 (19), 6298–6305.
Wang, X., Shi, H., Szanyi, J., 2017. Controlling selectivities in CO2 reduction through mechanistic understanding. Nature Commun. 8 (1), 513.
Wang, W., Wang, S., Ma, X., Gong, J., 2011. Recent advances in catalytic hydrogenation of carbon dioxide. Chem. Soc. Rev. 40 (7), 3703–3727.
Yu, Y., Bian, Z., Wang, J., Wang, Z., Tan, W., Zhong, Q., Kawi, S., 2021. Co2 hydrogenation to CH4 over hydrothermal prepared ceria-nickel catalysts: Performance and mechanism study. Catalysis Today.
Zhang, X., House, S.D., Tang, Y., Nguyen, L., Li, Y., Opalade, A.A., Yang, J.C., Sun, Z., Tao, F.F., 2018b. Complete oxidation of methane on NiO nanoclusters supported on CeO2 nanorods through synergistic effect. ACS Sustain. Chem. Eng. 6 (5), 6467–6477.
Zhang, G., Li, Y., Hou, Z., Xv, J., Wang, Q., Zhang, Y., 2018a. Research on the synergistic doped effects and the catalysis properties of Cu2+ and Zn2+ co-doped CeO2 solid solutions. J. Solid State Chem. 264, 148–155.
Zhao, K., Wang, L., Moioli, E., Calizzi, M., Züttel, A., 2019. Identifying reaction species by evolutionary fitting and kinetic analysis: An example of CO2 hydrogenation in DRIFTS. J. Phys. Chem. C 123 (14), 8785–8792.
Zheng, Y., Zhang, W., Li, Y., Chen, J., Yu, B., Wang, J., Zhang, L., Zhang, J., 2017. Energy related CO2 conversion and utilization: advanced materials/nanomaterials, reaction mechanisms and technologies. Nano Energy 40, 512–539.
Zhou, G., Barrio, L., Agnoli, S., Senanayake, S.D., Evans, J., Kubacka, A., Estrella, M., Hanson, J.C., Martínez-Arias, A., Fernández-García, M., 2010. High activity of Ce1- xNixO2- y for H2 production through ethanol steam reforming: tuning catalytic performance through metal–oxide interactions. Angew. Chem., Int. Ed. 49 (50), 9680–9684.
Zu, D., Wang, H., Lin, S., Ou, G., Wei, H., Sun, S., Wu, H., 2019. Oxygen-deficient metal oxides: Synthesis routes and applications in energy and environment. Nano Res. 12 (9), 2150–2163.